Advances in Applied Mathematics and Mechanics
Adv. Appl. Math. Mech., Vol. **5**, No. 6, pp. 846-856

DOI: 10.4208/aamm.2013.m132
December 2013

Flow Characteristics of Flapping Motion of a Plane Water Jet Impinging onto Free Surface

Liqing Zhao and Jianhong Sun*

College of Aerospace Engineering, Nanjing University of Aeronautics and Astronautics, 29 Yudao Street, Nanjing 210016, Jiangsu, China

Received 6 March 2013; Accepted (in revised version) 18 April 2013

Available online 6 September 2013

Abstract. A submerged turbulent plane jet in shallow water impinging vertically onto the free surface will produce a large-scale flapping motion when the jet exit velocity is larger than a critical one. The flapping phenomenon is verified in this paper through a large eddy simulation where the free surface is modeled by volume of fluid approach. The quantitative results for flapping jet are found to be in good agreement with available experimental data in terms of mean velocity, flapping-induced velocity and turbulence intensity. Results show that the flapping motion is a new flow pattern with characteristic flapping frequency for submerged turbulent plane jets, the mean centerline velocity decay is considerably faster than that of the stable impinging jet without flapping motion, and the flapping-induced velocities are as important as the turbulent fluctuations.

AMS subject classifications: 76D25

Key words: Turbulent plane jet, flapping motion, volume of fluid, large eddy simulation.

1 Introduction

For a submerged turbulent plane jet in shallow water impinging vertically onto the free surface, the jet will be self-excited into a flapping oscillation when the jet velocity, exiting the jet orifice, exceeds a critical value. One important characteristic of the flapping jet is to enhance mixing by flapping-induced Reynolds stress [1].In some cases, the instability of jet can be utilized to enhance the dilution. There is therefore a considerable interest in the design, performance and flow control of diffusers or mixers in chemical engineering, environmental engineering, and so on.

The flapping motion is a transverse oscillation of turbulent plane jet impinging onto free surface. A few parametric studies have been done to characterize the onset of flapping instability. Madarame et al. [2] established a relation between the flapping frequency

*Corresponding author.
Email: zhaoliqing@nuaa.edu.cn (L. Q. Zhao), jhsun@nuaa.edu.cn (J. H. Sun)

and the water depth. Wu et al. [3] performed experiments to delineate the critical jet exit velocity and the jet flapping frequency. All the experimental results in [2] and [3] were presented in dimensional form. Hsu et al. [4] and Sun [5] provided more general dimensionless parametric relations for the onset of flapping instability. In [4] and [5], the critical jet exit velocity W_{oc} was found to increase linearly with the water depth H and to decrease with the square root of the jet orifice width d. Meanwhile, the critical flapping frequency, f_0, was found to decrease with the root square of the water depth H, that is $f_0 \propto \sqrt{g/H}$. On the other hand, there remain debates on the mechanics of flapping motion. Hsu et al. [4] suggested that the flapping behavior was attributed to the self-excited jet instability, associated with the pressure restoring force increased by surface deformation due to gravity. However, in earlier research work, the flapping behavior was confirmed as the unstable motion due to the coherent turbulent structure [6,7]. Recently, Espa et al. [8] conducted experiments and smoothed particle hydrodynamics simulation to study the instability of a vertical plane jet introduced from the bottom of a finite depth laterally-confined water environment. It should be noted that the flow region in [8] was lateral confined and the ratio of water depth to orifice width was too small to reach the self-similar regime [9] for a submerged plane jet.

There are several kinds of self-induced oscillations coupled with jet flow and relatively few investigations have been conducted on them. The impingement of turbulent plane jets, upon an edge of a solid plate (a wedge of zero degree) in parallel to the jet flow was studied by Rockwell [10] and analyzed numerically by Ohring [11]. Ohring [11] predicted that the flapping oscillation of the impinging jet occurs at the subharmonic mode associated with the coherent large eddies. Gutmark et al. [12] studied the impingement of a plane jet onto a solid plate normal to the jet flow (a wedge of 180 degree) and did not detect any subharmonic transverse oscillations of the jets. Recently, the velocity oscillation phenomena in the far field region for plane jet at low Reynolds number was studied by Zhao et al. [13]. In comparison, the transverse flapping oscillation of turbulent jets in shallow water and more generally the detailed flow characteristics in this condition have so far received little attention in the specialized literature: only few experimental works [1–5,8] and very little numerical study [8,14] have addressed this topic.

In this paper, a large eddy simulation (LES) technique coupled with the volume of fluid (VOF) interface capturing method is utilized to investigate the flow characteristics of flapping motion. The purpose is to achieve an improved understanding of some of the fundamental characteristics in this flow, including the mean centerline velocity decay, flapping-induced velocities and frequency of the flapping motion.

2 Governing equations and numerical methodology

Large eddy simulation is implemented in the present work for turbulence closure, in which large-scale motions are explicitly calculated and the eddies with scale smaller than the grid or filter size are modeled to represent the effects of unresolved motions on re-

solved scale. The three-dimensional time dependent space filtered Navier-Stokes (N-S) equations coupled with volume of fluid (VOF) interface capturing equation can be written as [15]

$$\overline{\rho}\Big(\frac{\partial\widetilde{\boldsymbol{u}}}{\partial t}+\widetilde{\boldsymbol{u}}\cdot\bigtriangledown\widetilde{\boldsymbol{u}}\Big)=-\nabla\overline{p}+\overline{\rho}\boldsymbol{g}+\nabla\cdot(\overline{\mu}[\nabla\widetilde{\boldsymbol{u}}+\nabla^T\widetilde{\boldsymbol{u}}])+\boldsymbol{F}_{ST}(\overline{C})-\nabla\cdot\tau^{SGS}, \tag{2.1a}$$

$$\nabla\cdot\widetilde{\boldsymbol{u}}=0, \tag{2.1b}$$

$$\frac{\partial\overline{C}}{\partial t}+\widetilde{\boldsymbol{u}}\cdot\bigtriangledown\overline{C}=0, \tag{2.1c}$$

where an overbar denotes the spatial filter and a tilde represents the Favre filter, i.e., $\widetilde{\Phi}=\overline{\rho\Phi}/\overline{\rho}$. The variable $\overline{\rho}$ is the volume mass, $\widetilde{\boldsymbol{u}}$ velocity, $\overline{p}$ pressure, $\boldsymbol{g}$ the gravitational acceleration, $\overline{\mu}$ the dynamic viscosity, F_{ST} the surface tension force and $\overline{C}$ the volume fraction. Through Eq. (2.1c), the volume fraction $\overline{C}$ is advected with the fluid velocity $\widetilde{\boldsymbol{u}}$ and the evolution of either phase is known. The piecewise linear interface construction (PLIC) method is employed to construct the interface [16]. Note that the Favre filtering is equal to the conventional spatial filter at locations where the fluid density is constant. When the filtered volume function $\overline{C}$ is not constant, the filtered density $\overline{\rho}$ and viscosity $\overline{\mu}$ can be prescribed by

$$\overline{\rho}=\overline{C}\rho^1+(1-\overline{C})\rho^0, \tag{2.2a}$$

$$\overline{\mu}=\overline{C}\mu^1+(1-\overline{C})\mu^0. \tag{2.2b}$$

The variables with superscripts 1 and 0 refer to variables in the phase of water and air, respectively. Sub-grid term in (2.1a) is defined as

$$\tau^{SGS}=\overline{\rho\boldsymbol{u}\boldsymbol{u}}-\overline{\rho}\widetilde{\boldsymbol{u}}\widetilde{\boldsymbol{u}}. \tag{2.3}$$

In the present study, the Smagorinsky-Lilly model was used to model the sub-grid scale (SGS) stress tensor, shown as,

$$\tau^{SGS}=-\mu_t(\nabla\widetilde{\boldsymbol{u}}+\nabla^T\widetilde{\boldsymbol{u}})=-2\mu_t\widetilde{\boldsymbol{S}}, \tag{2.4a}$$

$$\widetilde{S}_{ij}=\frac{1}{2}\Big(\frac{\partial\widetilde{u}_i}{\partial x_j}+\frac{\partial\widetilde{u}_j}{\partial x_i}\Big), \tag{2.4b}$$

where $\mu_t=\overline{\rho}L_s^2|\widetilde{\boldsymbol{S}}|$ is the SGS viscosity, and $|\widetilde{\boldsymbol{S}}|=\sqrt{2\widetilde{S}_{ij}\widetilde{S}_{ij}}$. L_s is the length scale and is defined as $L_s=\min(kd,C_s\Delta)$ with $k=0.42$. The variable d is the distance to the closest wall. The value of Smagorinsky constant C_s is chosen as 0.1 in the present study. Δ, the local grid scale, is computed according to the volume of the computational cell by $\Delta=(\Delta_x\Delta_y\Delta_z)^{1/3}$.

The governing equations are numerically solved by SIMPLE method [17]. In Eq. (2.1a), a continuum surface force model proposed by Brackbill et al. [18] is implemented for the treatment of the surface tension effects. Spatial discretization is achieved using a

second-order-accurate central scheme. Temporal integration of the transient terms is performed by a second-order-accurate implicit scheme. This numerical strategy has already been applied with success to a wide range of turbulent shear flows such as jets in cross-flow [19,20] and the temporal mixing layer [21]. We have carefully examined the physical model and numerical approach used in this study and verified that the calculated results are reliable.

The flapping motion is a large-scale transverse oscillation. In accordance with Reynolds & Hussain [22], the space filtered velocity of flapping jet can be decomposed into three components, shown as,

$$\widetilde{u}_i = \langle \widetilde{u}_i \rangle + \widehat{u}_i + u_i', \tag{2.5}$$

where $\langle \widetilde{u}_i \rangle$ is the time-averaged contribution, $\widehat{u}_i$ is the flapping-induced periodic contribution and u_i' corresponds to the contribution of turbulent motion. Straightforward time averaging determines $\langle \widetilde{u}_i \rangle$. Then, the flapping-induced component can be decomposed in term of Fourier series as:

$$\widehat{u}_i = \sum_{n=1}^{N} |\widehat{u}_{i,n}| \sin(2n\pi f_0 t + \phi_{\widehat{u}_{i,n}}), \tag{2.6}$$

where f_0 denotes the frequency of flapping motion, $|\widehat{u}_{i,n}|$ and $\phi_{\widehat{u}_{i,n}}$ denote the amplitude and phase angle of the nth harmonic component $\widehat{u}_{i,n}$. Then we have,

$$\langle \widehat{u}_{i,n}^2 \rangle = \frac{1}{2} |\widehat{u}_{i,n}|^2. \tag{2.7}$$

As a result, the turbulence intensity and Reynolds shear stress can be obtained by

$$\langle u_i' u_j' \rangle = \langle (\widetilde{u}_i - \langle \widetilde{u}_i \rangle)(\widetilde{u}_j - \langle \widetilde{u}_j \rangle) \rangle - \sum_{n=1}^{N} \langle \widehat{u}_{i,n} \widehat{u}_{j,n} \rangle. \tag{2.8}$$

3 Results and discussion

3.1 Set-up of problem

As shown in Fig. 1, water enters vertically into the computational domain of $H_x \times H_y \times H_z$ with uniform jet exit velocity W_o from a bottom slit. The slit is centered on the lower boundary of the computational domain with width d. In the Cartesian coordinate system, the coordinate origin is set at the center of the slit and z is measured upward from the jet orifice. The water depth and the jet orifice width are maintained at $H = 0.1$m and $d = 0.002$m. Based on empirical formula in [4] and [5], the corresponding critical jet exit velocity W_{oc} is about 1.31m/s. In order to reproduce the flapping motion, the jet exit velocity W_o is chosen as 1.72m/s in the present study, which gives Reynolds number of $Re = W_o d/\nu = 2970$, where ν is the fluid viscosity. For the purpose of maintaining

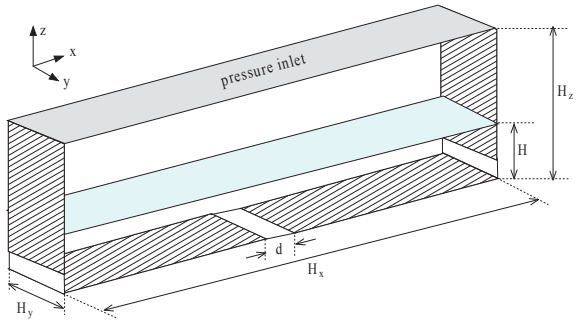

Figure 1: Computational domain.

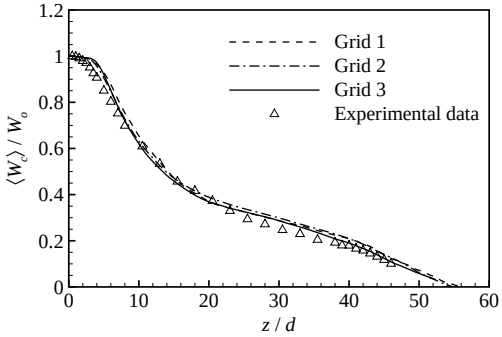

Figure 2: Comparison of the calculated mean centerline velocity with experimental data.

water level at constant in simulation, two velocity outlets are applied at the two end of the tank bottom. The upper boundary condition for air in the calculation is set to inlet condition with same pressure. Periodic boundary conditions are applied in the spanwise (y) direction. Other boundaries are set to solid wall with no-slip boundary condition.

The three-dimensional hexahedral grid was generated using Gridgen software. Three typical grids denoted by Grids 1-3 are listed in Table 1. Fig. 2 shows the decay of the calculated mean centerline velocity $\langle \widetilde{W_c} \rangle / W_o$ and its comparison with the experimental data [5]. It is exhibited that the result for Grid 3 compares well with the experimental data. To make the prediction accurate, the results given below are calculated using the parameters in Case 3 and the time step is set as $0.1d/W_o$

Table 1: Validation of grid resolution.

Grid	$H_x \times H_y \times H_z$	Mesh size
Grid 1	$30H \times 4d \times 1.8H$	$250 \times 33 \times 173$
Grid 2	$30H \times 4d \times 5H$	$273 \times 33 \times 200$
Grid 3	$30H \times 10d \times 5H$	$273 \times 81 \times 200$

3.2 Flow characteristics

The calculated variation of the mean centerline velocity $\langle\widetilde{W_c}\rangle/W_o$ is given for flapping jet in Fig. 3, along with measured data [5]. Also included in the figure are experimentally and numerically determined results for stable jet without flapping motion ($W_o=1.21$m/s when $H/d=50$). The present results based on LES simulation fit well with experimental data. On the other hand, as shown in Fig. 3, the decay rule for flapping jet is about -0.8, which is apparently faster than that for stable jet without flapping motion.

To further understand the flow characteristics of flapping jet, Fig. 4 illustrates the resulting transverse distribution $\langle\widetilde{u}\rangle/W_o$ and longitudinal distribution $\langle\widetilde{w}\rangle/W_o$ at z/d=5, 15 and 20. As expected, the longitudinal velocity $\langle\widetilde{w}\rangle/W_o$ at the jet centerline decreases and the width of the jet increases downstream. It is observed that the numerical results are in agreement with the experimental data [5].

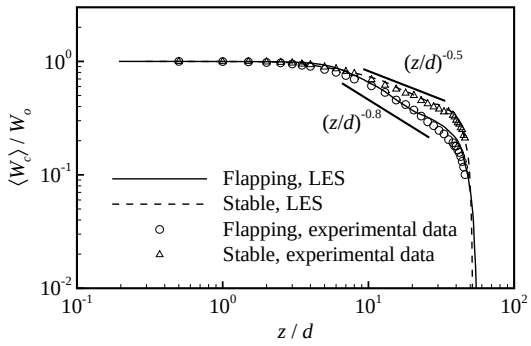

Figure 3: Decay of mean velocity along jet centerline.

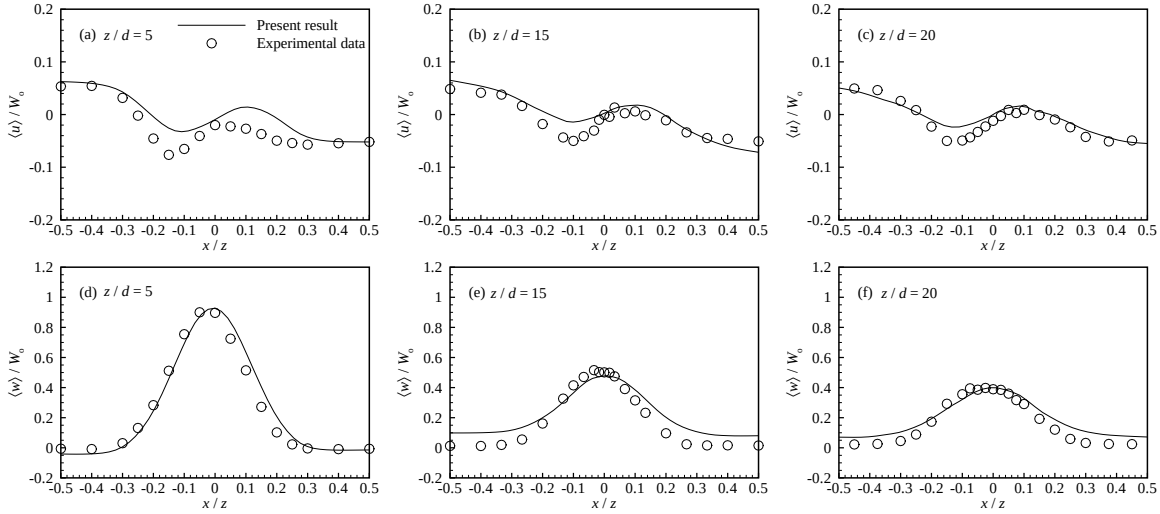

Figure 4: The distribution of the mean transverse and longitudinal velocities.

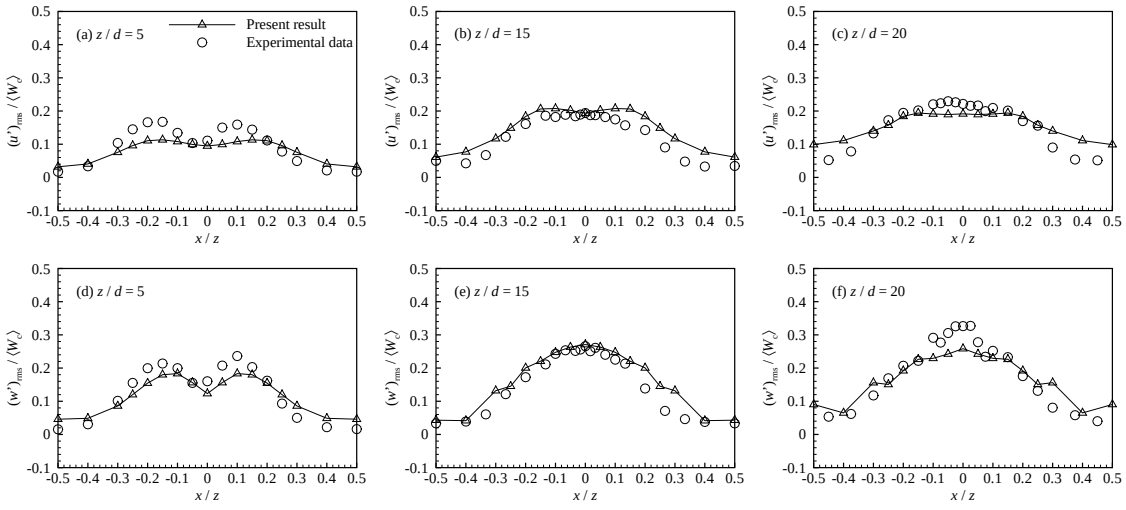

Figure 5: The distribution of transverse and longitudinal turbulence intensities.

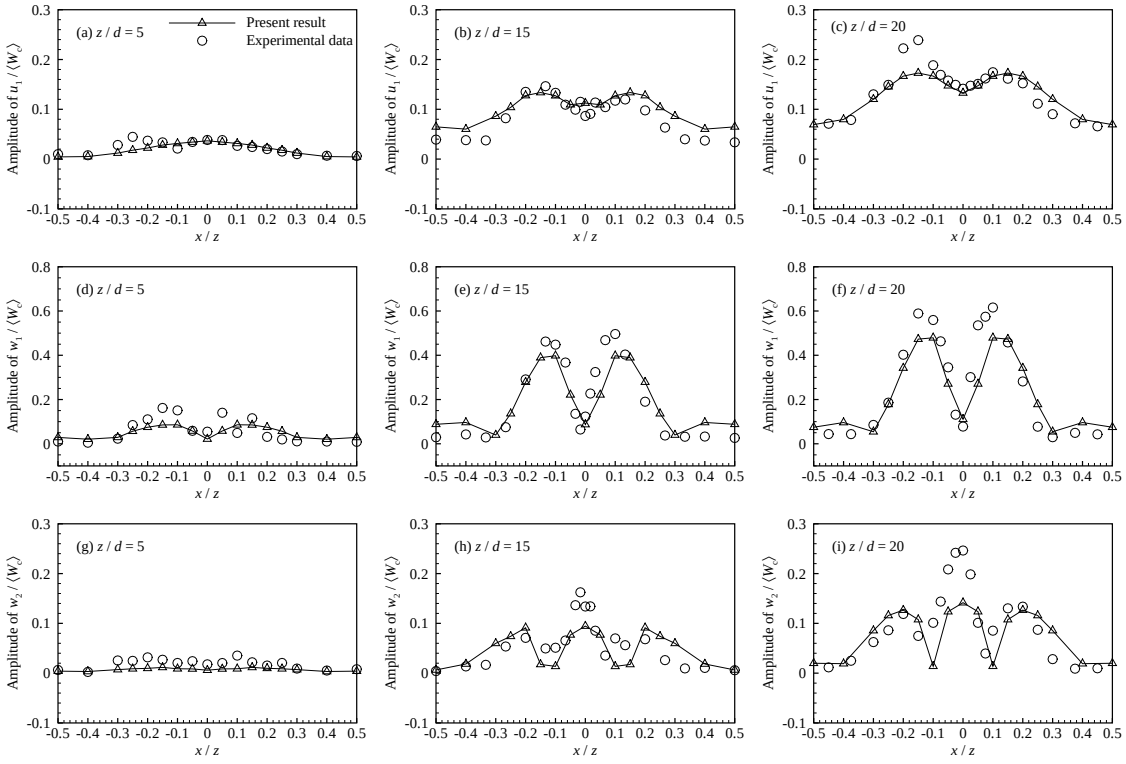

Figure 6: The amplitude of flapping-induced transverse and longitudinal velocity components.

Figs. 5(a)-(f) are graphs showing comparisons of transverse ($\sqrt{u'^2}/\langle\widetilde{W}_c\rangle$) and longitudinal ($\sqrt{w'^2}/\langle\widetilde{W}_c\rangle$) turbulence intensities between the experimental and numerical results at z/d=5, 15 and 20. Here $\sqrt{u'^2}$ and $\sqrt{w'^2}$ are the root-mean-square values of the velocity fluctuations in the transverse and longitudinal directions, respectively. Both turbulence intensities exhibit similar behavior in the region close to the jet exit (Figs. 5(a) and (d)), namely, dips are found at the centerline and maximum values exist in the shear layer region. Fig. 6 shows the comparisons of amplitude of flapping-induced velocity components between experimental and numerical results at $z/d=5$, 15 and 20. It is observed that the peak value of $|\widehat{w}_1/\langle\widetilde{W}_c\rangle|$ at each z/d is higher than that of either $|\widehat{u}_1/\langle\widetilde{W}_c\rangle|$ or $|\widehat{w}_2/\langle\widetilde{W}_c\rangle|$. On the other hand, the peak value of $|\widehat{w}_1/\langle\widetilde{W}_c\rangle|$ at $z/d=15$ (Fig. 6(e)) is a little bit larger than that of the longitudinal turbulence intensity (Fig. 5(e)). This indicates that the flapping-induced components are as important as the turbulence intensities for flapping jet. Both the calculated results in Figs. 5 and 6 are in good agreement with the experimental data [5].

3.3 Frequency characteristics

Fig. 7 shows the contours of instantaneous velocity magnitude normalized with the jet exit velocity (W_o) of the flapping jet at $y=0$ in one-half period $T/2$. Note that the starting time in Fig. 7 is arbitrary. The oscillation of surface deformation is observed to synchronize with the jet flapping motion. As shown in Fig. 7(a), the jet flaps to the right maximum displacement location at $t=0$. At $t=T/4$, jet oscillates backward to the center plane above the jet orifice as shown in Fig. 7(b). Fig. 7(c) shows that the plane jet continues to flap towards the left of the jet orifice and reaches the left maximum displacement at $t=T/2$ to complete one-half cycle of oscillation.

To obtain the frequency of the flapping motion, the power spectral densities of centerline velocities, $\widetilde{u}$ and $\widetilde{w}$ at $z/d=28$ are shown in Fig. 8. The non-dimensional frequencies, $St=fd/W_o$ for transverse velocity and longitudinal velocity are about 0.0019 and 0.0038, respectively. The corresponding frequencies obtained based on laser Doppler velocimeter (LDV) measurements at the same position in [5] were 0.002 and 0.004, respectively. The flapping frequencies in the present simulation are in good agreement with the ex-

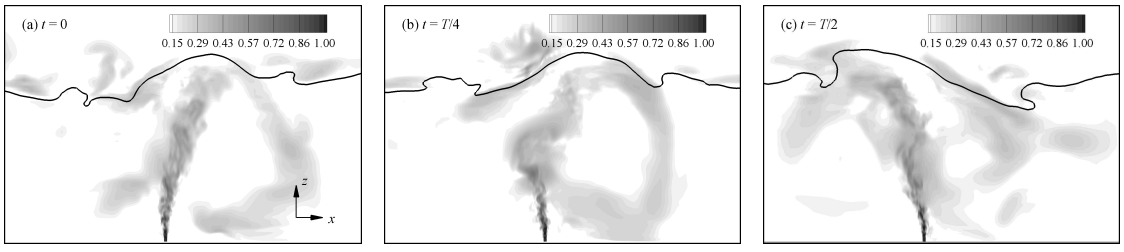

Figure 7: Visualization of instantaneous non-dimensional velocity magnitude $|\widetilde{\mathbf{u}}|/W_o$ at $y=0$ in one-half period. Solid line represents the free surface.

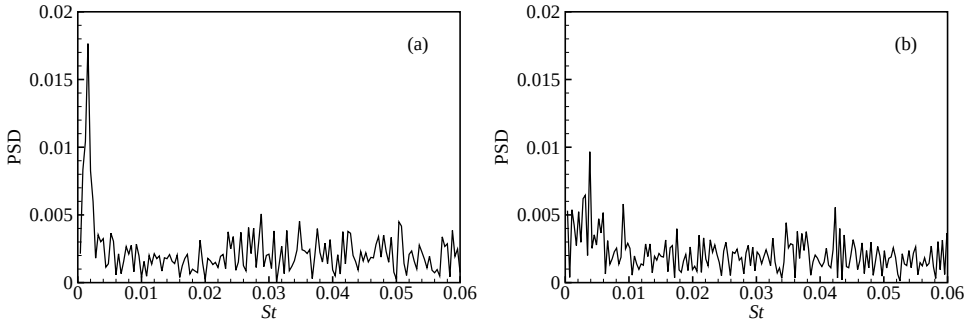

Figure 8: The power spectral densities of centerline velocities at $z/d=28$: (a) $\widetilde{u}$, (b) $\widetilde{w}$.

perimental measurement. Meanwhile, the frequency of longitudinal velocity oscillation at the jet centerline is twice of the transverse oscillation. This is merely a consequence of large amplitude jet flapping motion. It should be noted that the frequency of flapping motion is two orders of magnitude lower than that associated with the coherent structures in a jet identified by Crow & Champagne [23]. In [23], the dimensionless frequency of the coherent structures in self-similar region is found to be 0.3. The lower magnitude of the Strouhal number of flapping jet suggests that the frequency is associated with a larger motion of the jet as a whole, rather than with the coherent structure within the jet.

4 Conclusions

For a submerged turbulent plane jet in shallow water impinging vertically onto the free surface, the jet will be self-excited into a flapping oscillation when the jet velocity, exiting the jet orifice, exceeds a critical value. In this study, volume of fluid approach coupled with a large eddy simulation is applied to predict the flow characteristics of the flapping jet. The quantitative results for flapping jet are found to be in good agreement with available experimental data in terms of mean velocity, flapping-induced velocity and turbulent fluctuation. Results show that the flapping motion is a new flow pattern for submerged turbulent plane jets with characteristic flapping frequency. The frequency of longitudinal velocity oscillation at the jet centerline is found twice of that of the transverse oscillation. Results also show that the mean centerline velocity decay is considerably faster than that of the stable impinging jet without flapping motion. In addition, the magnitudes of flapping-induced velocities have almost the same order of that of the turbulent fluctuation, which indicates that the flapping-induced components are as important as the turbulent fluctuation for flapping jet.

Acknowledgments

The work was supported by National Natural Science Foundation of China (Grant No. 10472046), the Priority Academic Program Development of Jiangsu Higher Edu-

cation Institutions, grants from the Postgraduate Research and Innovation Project of Jiangsu Province (Grant No. CX08B_035) and PhD Thesis Innovation and Excellence Fund of NUAA (Grant No. BCXJ08-01).

References

[1] J. H. SUN, L. Q. ZHAO AND C. T. HSU, *Theoretical analyses on flapping motion of submerged turbulent plane jets*, Mod. Phys. Lett. B, 19 (2005), pp. 1471–1474.
[2] H. MADARAME AND M. IIDA, *Mechanism of jet-flutter: self-induced oscillation of an upward plane jet impinging on a free surface*, JSME Int. J. B–Fluid T., 41 (1998), pp. 610–617.
[3] S. WU, N. RAJARATNAM AND C. KATOPODIS, *Oscillating vertical plane turbulent jet in shallow water*, J. Hydraul. Res., 36 (1998), pp. 229–234.
[4] C. T. HSU, J. KUANG AND J. H. SUN, *Flapping instability of vertically impinging turbulent plane jets in shallow water*, J. Eng. Mech., 127 (2001), pp. 411–420.
[5] J. H. SUN, Flapping Turbulent Plane Jets in Shallow Water and Interacting with Surface Waves, PhD thesis, The Hong Kong University of Science and Technology, Hong Kong, China, 2001.
[6] V. W. GOLDSCHMIDT AND P. BRADSHAW, *Flapping of a plane jet*, Phys. Fluids, 16 (1973), pp. 354–355.
[7] J. C. D. GORTARI AND V. W. GOLDSCHMIDT, *The apparent flapping motion of a turbulent plane jet: further experimental results*, J. Fluids Eng., 103 (1981), pp. 119–126.
[8] P. ESPA, S. SIBILLA AND M. GALLATI, *SPH simulations of a vertical 2-D liquid jet introduced from the bottom of a free surface rectangular tank*, Adv. Appl. Fluid Mech., 3 (2008), pp. 105–140.
[9] J. KUANG, C. T. HSU AND H. H. QIU, *Experiments on vertical turbulent plane jets in water of finite depth*, J. Eng. Mech., 127 (2001), pp. 18–26.
[10] D. ROCKWELL, *Oscillations of impinging shear layer*, AIAA J., 21 (1983), pp. 645–664.
[11] S. OHRING, *Calculation of self-excited impinging jet flow*, J. Fluid Mech., 163 (1986), pp. 69–98.
[12] E. GUTMARK, M. WOLFSHTEIN AND I. WYGNANSKI, *The plane turbulent impinging jet*, J. Fluid Mech., 88 (1978), pp. 737–756.
[13] L. Q. ZHAO, J. H. SUN AND C. Y. XU, *Flow field analyses of plane jet at low Reynolds number using lattice Boltzmann method*, Transactions of Nanjing University of Aeronautics & Astronautics, 29 (2012), pp. 199–206.
[14] L. Q. ZHAO, J. H. SUN AND P. P. ZHOU, *Numerical simulation flapping motion of submerged plane water jets*, Mod. Phys. Lett. B, 23 (2009), pp. 329–332.
[15] J. LAROCQUE, N. RIVIÈRE, S. VINCENT, D. REUNGOAT, J. P. FAURE, J. P. HELIOT, J. P. CALTAGRIONE AND M. MOREAU, *Macroscopic analysis of a turbulent round liquid jet impinging on an air/water interface in a confined medium*, Phys. Fluids, 21 (2009), 065110.
[16] D. GUEYFFIER, J. LI, A. NADIM, R. SCARDOVELLI AND S. ZALESKI, *Volume-of-fluid interface tracking with smoothed surface stress method for three-dimensional flows*, J. Comput. Phys., 152 (1999), pp. 423–456.
[17] S. V. PATANKAR AND D. B. SPALDING, *A calculation procedure for heat, mass and momentum transfer in three-dimensional parabolic flows*, Int. J. Heat Mass Tran., 15 (1972), pp. 1787–1806.
[18] J. U. BRACKBILL, B. D. KOTHE AND C. ZEMACH, *A continuum method for modeling surface tension*, J. Comput. Phys., 100 (1992), pp. 335–354.
[19] P. MAJANDER AND T. SIIKONEN, *Large-eddy simulation of a round jet in a cross-flow*, Int. J. Heat Fluid Fl., 27 (2006), pp. 402–415.

[20] W. P. JONES AND M. WILLE, *Large-eddy simulation of a plane jet in a cross-flow*, Int. J. Heat Fluid Fl., 17 (1996), pp. 296–306.
[21] B. VREMAN, B. GEURTS AND H. KUERTEN, *Comparison of numerical schemes in large-eddy simulation of the temporal mixing layer*, Int. J. Numer. Meth. Fl., 22 (1996), pp. 297–311.
[22] W. C. REYNOLDS AND A. K. M. F. HUSSAIN, *The mechanics of an organized wave in turbulent shear flow, part 3: theoretical models and comparisons with experiments*, J. Fluid Mech., 54 (1972), pp. 263–288.
[23] S. C. CROW AND F. H. CHAMPAGNE, *Orderly structure in jet turbulence*, J. Fluid Mech., 48 (1971), pp. 547–591.